


# Process design for the manufacturing of soft X-ray gratings in single-crystal diamond by high-energy heavy-ion irradiation

G. García<sup>1,a</sup> , M. Martín<sup>1</sup>, M. D. Ynsa<sup>1,2</sup>, V. Torres-Costa<sup>2</sup>, M. L. Crespillo<sup>1</sup>, M. Tardío<sup>3</sup>, J. Olivares<sup>1,4</sup>, F. Bosia<sup>5</sup>, O. Peña-Rodríguez<sup>6</sup>, J. Nicolas<sup>7</sup>, M. Tallarida<sup>7</sup>

<sup>1</sup> Centro de Microanálisis de Materiales (CMAM), Universidad Autónoma de Madrid (UAM), Cantoblanco, 28049 Madrid, Spain

<sup>2</sup> Departamento de Física Aplicada, Universidad Autónoma de Madrid, 28049 Madrid, Spain

<sup>3</sup> Departamento de Física, Universidad Carlos III de Madrid, Avda. Universidad 30, 28911 Leganés, Madrid, Spain

<sup>4</sup> Instituto de Óptica, Consejo Superior de Investigaciones Científicas (CSIC), C/Serrano 121, 28006 Madrid, Spain

<sup>5</sup> Department of Applied Science and Technology, Politecnico Di Torino, Turin, Italy

<sup>6</sup> Instituto de Fusión Nuclear “Guillermo Velarde”, Universidad Politécnica de Madrid, C/ José Gutiérrez Abascal 2, 28006 Madrid, Spain

<sup>7</sup> ALBA Synchrotron Light Source (CELLS-ALBA), Cerdanyola del Vallès, 08290 Barcelona, Spain

Received: 17 June 2022 / Accepted: 2 October 2022

© The Author(s) 2022

**Abstract** This paper describes in detail a novel manufacturing process for optical gratings suitable for use in the UV and soft X-ray regimes in a single-crystal diamond substrate based on highly focused swift heavy-ion irradiation. This type of grating is extensively used in light source facilities such as synchrotrons or free electron lasers, with ever-increasing demands in terms of thermal loads, depending on beamline operational parameters and architecture. The process proposed in this paper may be a future alternative to current manufacturing techniques, providing the advantage of being applicable to single-crystal diamond substrates, with their unique properties in terms of heat conductivity and radiation hardness. The paper summarizes the physical principle used for the grating patterns produced by swift heavy-ion irradiation and provides full details for the manufacturing process for a specific grating configuration, inspired in one of the beamlines at the ALBA synchrotron light source, while stressing the most challenging points for a potential implementation. Preliminary proof-of-concept experimental results are presented, showing the practical implementation of the methodology proposed herein.

## 1 Introduction

Swift heavy-ion irradiation of single-crystal diamond, as is the case for a wide variety of materials, generates an energy deposition depth profile that may lead, with proper choice of the ion beam parameters, to intensive structural damage at a buried layer inside the sample, whereas the sample surface remains practically unaffected [1–3]. One of the outcomes of such an irradiation scheme is that the heavily damaged volume buried inside the sample generates a swelling effect transmitted to the sample surface [4–7], in such a way that a topography is generated on the structurally intact surface reflecting the amount of damage accumulated beneath. The effect has been shown to be suitable for the generation of customized three-dimensional surface patterns by irradiation with a proper mask [8], based on the knowledge accumulated in previous works on the response of single-crystal diamond to irradiation under different conditions [3]. A similar effect has also been seen using low-energy heavy ions and a diffraction optical element has been manufactured using high-dose implantation in diamond of 40 keV boron ions through a surface mask [9].

This paper describes the full process of manufacturing of a preliminary device based on this principle, with the aim of assessing the practical difficulties to be met, as an initial step before possible implementation. Preliminary proof-of-concept experimental results are included, to validate the main practical aspects of the proposed procedure.

The chosen device is a UV/soft X-ray grating. Gratings operating as part of beamline monochromators in facilities such as synchrotrons or free electron lasers in the UV to soft X-ray regimes are made by mechanically patterning a given substrate [10], with proper parameters to filter the incoming polychromatic light and allow through a monochromatic beam of the desired wavelength at each moment during the experiment [11]. The evolution of light sources during the past decade and the plans for the early future involve an explosive growth of light yields and thereby of heat load in the different optical elements. Therefore, it is expected that the heat load challenge should continue growing and eventually lead to the need of considering alternative approaches, such as using single-crystal diamond as an alternative substrate. Two main difficulties may be considered for this option to become feasible: availability of diamond single crystals with large enough size at a reasonable cost and availability of a method to obtain grating patterns on the diamond surface. This paper focuses only on the latter.

<sup>a</sup> e-mail: [ggarcia@cells.es](mailto:ggarcia@cells.es) (corresponding author)

The paper is organized as follows: Sect. 2 describes a typical target grating geometry, in which the subsequent work will be inspired; Sect. 3 recalls the basic physical principles and expressions needed to understand and quantify the damage process giving rise to the grating pattern and provides the calculation results in illustrative examples; Sect. 4 gives first experimental results with a simplified geometry, conceptually similar to the one described in the previous sections; finally, Sect. 5 presents the conclusions and outlook, with particular attention to implementation challenges.

## 2 Target grating geometry

The grating geometry chosen for this work is adapted to the beamline BL20-LOREA [12], which has recently started operation at the ALBA synchrotron [13]. LOREA is a beamline designed to perform angle-resolved photoemission spectroscopy experiments for electronic characterization of complex materials. It works in the UV and soft X-ray wavelength regimes, with light supplied by a long-period helical undulator and filtered at a monochromator developed by ALBA. The first optical element is a mirror (part of the monochromator), followed by a grating. A total of four different gratings (with the option of adding a fifth one) are available and can be inserted into the beam by a motorized translation stage, to optimally cover the different spectral subranges targeted by the beamline. The photon total spectral range to be covered is 10–1000 eV. The thermal energy load at the grating stage is at a maximum level of 1 W, the highest power density being ca. 10 mW/mm<sup>2</sup>. Therefore, a Si substrate with proper water cooling is sufficient in this case. It is clear, though, that the evolution of synchrotron light sources and free electron lasers poses severe challenges to future grating technologies in terms of heat load. The LOREA grating geometry has thus been taken as a representative one for this work, wherein a diamond substrate could be the right option if the device could run under more severe heat load conditions.

The chosen grating geometry is that of the so-called xLEG grating (where xLEG stands for extra-low-energy grating). This grating covers the 10–35 eV X-ray energy range. The reference line density is 200 lines/mm and the groove profile is blazed, with a blaze angle of 1.5°. This type of profile has been chosen by optimizing diffraction efficiency and high harmonic rejection. In addition to the mentioned basic parameters, the grating has the feature of a smooth variation of line density along the grating length. Thereby, the line density follows a quadratic spatial dependence along the grating according to the formula

$$k(x) = k_0 + k_1x + k_2x^2 \quad (1)$$

where  $x$  is the position along the grating surface in the dispersive direction,  $k(x)$  is the local line density at point  $x$ , and the relevant parameters take the values  $k_0 = 200 \text{ mm}^{-1}$ ,  $k_1 = 53.73 \text{ mm}^{-1} \text{ m}^{-1}$ , and  $k_2 = 10.67 \text{ mm}^{-1} \text{ m}^{-2}$ . It may be easily seen that line density takes the reference value at the central part of the grating ( $x = 0$ ), whereas it deviates gradually from this value toward the grating edges. This configuration can optimize optics performance downstream of the beamline, considering chromatic aberration.

In this work, we have chosen a simplified geometry with the same type of features as the one described above. The period has been chosen as 20  $\mu\text{m}$  (i.e., 50 lines/mm), whereas the blaze angle has been taken to be 0.0625°. This value turns out to be a good choice, as it limits the total time of irradiation necessary to manufacture the grating and illustrates all the practical aspects of the method.

## 3 Procedure for grating manufacturing

Surface swelling  $h$  at an arbitrary point  $(x, y)$  of the sample surface may be quantified as

$$h(x, y) = b \int_0^{z_{\max}} \left[ 1 - \exp\left(-\Phi(x, y) \cdot \frac{S_n(z)}{a}\right) \right] dz \quad (2)$$

where  $h(x, y)$  is measured in distance units,  $\Phi(x, y)$  is the total ion fluence received at point  $(x, y)$  in ion/cm<sup>2</sup> units, and  $S_n(z)$  is the linear nuclear energy density deposition as a function of depth into the sample given in keV/nm, as obtained from the SRIM simulation package [14, 15]. Constants  $a$  and  $b$  have been determined by proper fitting to experimental data [3] and are characteristic of single-crystal diamond, wherein for the values of the electronic stopping force considered in this work swelling depends only on nuclear stopping, as indicated in Eq. (2). The corresponding values are  $a = (1.19 \pm 0.11) \times 10^{15} \text{ cm}^{-2} \text{ keV nm}^{-1}$  and  $b = 0.25 \pm 0.05$ . Notice that  $b$  has been chosen to be non-dimensional, so that  $h(x, y)$  retains the units of the depth integration variable  $z$ . In practice, it is frequent to work with  $z$  expressed in  $\mu\text{m}$ , whereas  $h(x, y)$  is typically expressed in nm.

In the grating patterns considered in this work, there is translational symmetry along the groove direction. Therefore, the implanted pattern is effectively one-dimensional and one of the two variables  $(x, y)$  may be dropped from (2) without loss of generality.

Once the material has been chosen as single-crystal diamond (which fixes the value of  $a$  and  $b$ ) and the type of ion and its energy are selected (which fixes  $S_n(z)$ ), formula (2) may be read as an integral equation in which, dropping the  $y$  variable,  $h(x)$  is fixed to a given grating target pattern, whereas  $\Phi(x)$  is the function to be solved for. The equation may be solved numerically, and therefore the target fluence profile is obtained. The manufacturing problem is now thus reduced to irradiating the sample with a given profile  $\Phi(x)$ .

**Fig. 1** Target grating profile (upper) and required fluence pattern (lower) to obtain it with a C ion beam at 9 MeV. The blaze angle is  $0.0625^\circ$

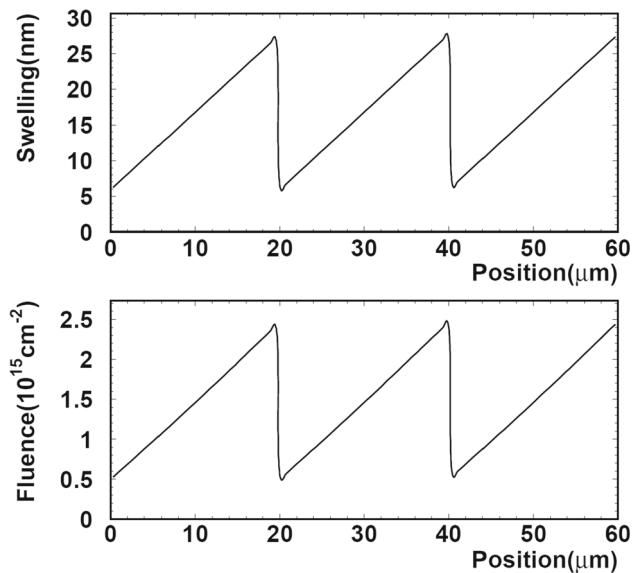


**Fig. 2** Target grating profile (upper) and required fluence pattern (lower) to obtain it with a C ion beam at 9 MeV. The blaze angle is  $1^\circ$

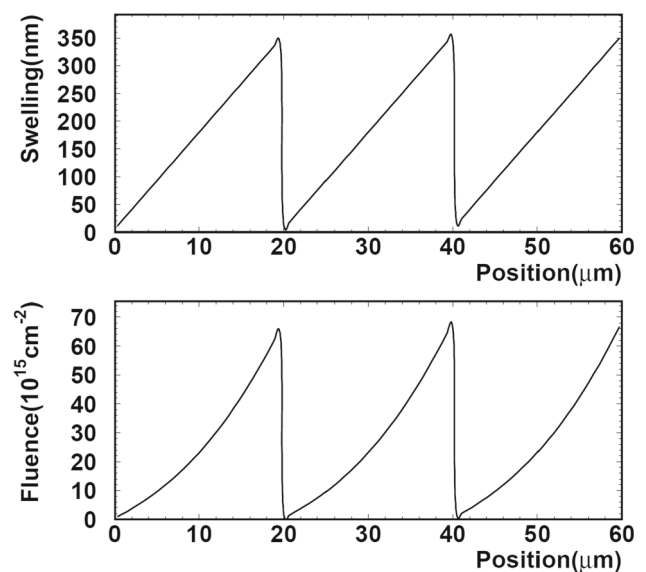


Figure 1 illustrates this by showing a given target grating profile  $h(x)$  and the corresponding fluence profile  $\Phi(x)$  required to generate it. We have chosen as an example a very small blaze angle ( $0.0625^\circ$ ) and a period of  $20 \mu\text{m}$ , as indicated in the previous section. Figure 2 replicates this calculation for a similar geometry, but involving a larger blaze angle ( $1^\circ$ ). These geometries have been chosen to illustrate the type of challenges to be met for cases similar to the xLEG grating of the LOREA beamline at ALBA, as defined above in this work. It may be observed that for very small blaze angles, which imply low maximum swelling values and thus very limited maximum fluence, the  $\Phi(x)$  plot looks practically linear, as it may be derived from Eq. (2) by assuming that the exponent of the integral is small for all values of the integration variable and performing a series expansion of the exponential. As the blaze angle increases, the maximum fluence becomes larger and the linear approximation is no longer accurate. In Fig. 2, one observes very clearly that the  $\Phi(x)$  is superlinear, to compensate for the first indications of damage saturation in the integrand of Eq. (2). In both cases, the fluence at the point of minimum swelling has been chosen to be larger than zero, as in practice setting a zero fluence target at a point of the sample would imply to scan the beam at infinite velocity. This minimum fluence value has been arbitrarily chosen as  $10^{14} \text{ ions/cm}^2$ , which corresponds to a swelling close to 1 nm, as detailed below.

The practical way we used to calculate  $\Phi(x)$  for the experimental implementation is described in the following steps:

- We assume a blaze geometry as a target, i.e.,  $h(x) = A + Bx$ . Notice that it is more practical to choose  $A > 0$ , so that the target fluence does not become zero at  $x = 0$ . As the aim of the experiment (see Sect. 4) was to demonstrate the feasibility of manufacturing a few grating lines, we worked with a fully periodic geometry, instead of a variable line density, as in the most general case.

- Equating our linear target profile for  $h(x)$  in Eq. (2), we derive with respect to  $x$  in both sides and then solve for  $\Phi'(x)$ , yielding

$$\Phi'(x) = \left(\frac{Ba}{b}\right) \int_0^{z_{\max}} \left[ S_n(z) \exp\left(-\Phi(x, y) \cdot \frac{S_n(z)}{a}\right) \right] dz \quad (3)$$

- Use (2) to obtain  $\Phi(0)$ , so that  $h(0) = A$ .
- Use (3) to integrate stepwise and thus obtain  $\Phi(x)$  for each value of  $x$ . Alternatively, these last three steps may be replaced by direct numerical inversion of the function (2) by building a lookup table and then interpolating.
- Set the irradiation program by scanning the beam on the sample in small steps along the  $y$  direction to a given desired width  $w$ , and then move the beam along  $x$  by a small step and scan again along  $y$ . Notice that the beam scan steps must be much smaller than the grating period, to obtain a quasi-continuous fluence deposition profile.
- Convert the desired value for  $\Phi(x, y)$  at each point to a discrete map with the beam charge value at each point by applying  $Q = \Phi w l q / N$ , where  $w$  and  $l$  are the width and length of one grating period, respectively,  $q$  is the charge state of the ion used for irradiation, and  $N$  is the number of lines scanned by the beam for each grating period.

As detailed below, in our experimental implementation we chose to scan a beam of micrometric dimensions in front of the sample. Alternatively, one may scan the sample with a static beam. The beam size must be smaller than the grating period, to limit the smoothing of the actual obtained geometry as compared to the ideal target one. This may be obtained by beam focusing, as in our case, or by a micrometric slit.

#### 4 Experimental results for a simplified geometry

For the first proof-of-concept experiment, we used an optical-grade single-crystal diamond sample,  $(3 \times 3 \times 0.3) \text{ mm}^3$  in size, (100) oriented and with two polished surfaces, supplied by Element Six [16]. The samples were classified as type IIa, corresponding to concentrations of N and B impurities below 1 ppm and 50 ppb, respectively.

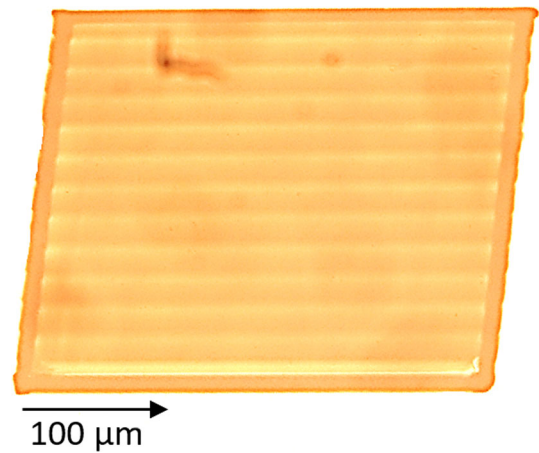
The implantations were performed at the CMAM microbeam line [17, 18], using a focused 9 MeV  $^{12}\text{C}^{+3}$  ion beam with a size of about  $5 \times 2 \mu\text{m}^2$  and a beam current of about 200 pA. The sample was implanted in frontal geometry, and the scan was performed pixel-by-pixel using a home-made software. The beam commenced its scan in the top left corner of the pattern scan area and then continued in the horizontal direction to the right, dropping to the next scan line when the right edge of the scan region was reached and returning to the left edge. The beam position to the next pixel was moved once the prescribed charge was achieved. Charge was integrated by means of an insulated sample holder.

The implanted pattern consisted of 12 blazed lines with a total width of 320  $\mu\text{m}$ . As the system was run without an accurate charge measurement and step scan calibration in this experiment, the blaze angle and the grating period, chosen to be at the level of a fraction of a degree and in the 10–20  $\mu\text{m}$  range, respectively, were effectively left as free parameters to be determined from experimental data post-irradiation characterization of the sample. The irradiation plan was like the one depicted in Fig. 1, therefore featuring a linear relationship between fluence and swelling. This geometry was chosen to limit the total fluence required for this first proof of principle experiment and to validate the possibility of generating ultra-shallow blaze angles. The irradiation plan was performed following the steps given in Sect. 3. The fluences, following the methodology of the previous sections, were calculated to vary between the values  $10^{14}$  ions/cm<sup>2</sup> and  $3 \times 10^{15}$  ions/cm<sup>2</sup>.

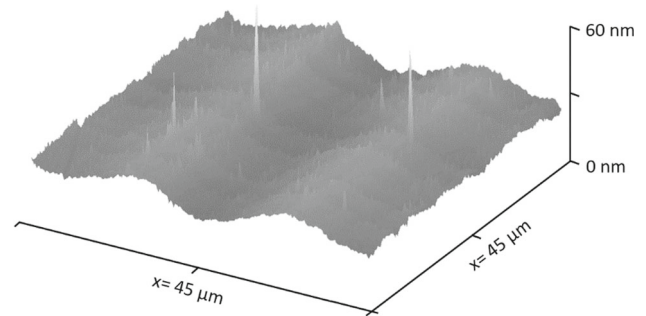
Figure 3 shows an optical microscope image of the irradiated sample, where the 12 lines may be seen very clearly, as diamond becomes dark upon ion irradiation with a sufficiently high fluence. The surface morphology of the sample after irradiation was measured by atomic force microscopy (AFM) with a commercial instrument from Park Systems XE-100 (Park Systems Corp., Suwon, Korea), under non-contact mode operating in air at room temperature. The cantilever dimensions are  $125 \times 30 \times 4 \mu\text{m}$ . Heavily doped silicon tips (910 M-ACTA) with aluminum coating 30 nm thick (force constant 37 N/m, resonance frequency 330 kHz) were used. The tip radius of curvature reported by the manufacturer is less than 10 nm. The acquisition was conducted using XEI's Park System software, and further analysis for image processing and measurements of the acquired data was performed using Gwyddion 2.59, a widely used, freely available open-source software package (<http://gwyddion.net/>). Samples were analyzed without any pre-treatment. The AFM three-dimensional images on five different regions of the sample with dimensions of  $45 \times 45 \mu\text{m}^2$  were taken under similar conditions: in air and at room temperature and at a scan rate of 0.5 Hz; 256 points per scan were recorded with the aim of getting enough statistical data points. The scanning direction was chosen along the grating dispersive direction, i.e., perpendicular to grating lines. The topography obtained by the irradiation program applied to the sample is shown in Fig. 4. The desired geometry was obtained with regular and reproducible patterns in the different parts of the irradiated area. A more quantitative view may be obtained as a greyscale map in Fig. 5.

Figure 6 provides three AFM line scans along the grating dispersive direction. Notice that the grating geometry is very reproducible. The experimental value for the period is very close to 20  $\mu\text{m}$ , and the blaze angle is slightly larger, but comparable to the value shown in Fig. 1. The actual pattern is clearly smoothed out with respect to the ideal grating geometry. This is due to the nonzero beam size as well as to the elastic behavior of the material, which would yield smoothed-out profiles even in the case of an ideal beam with a size much smaller than the grating period. SRIM predicts a lateral straggling of just around 100 nm for 9 MeV C ions

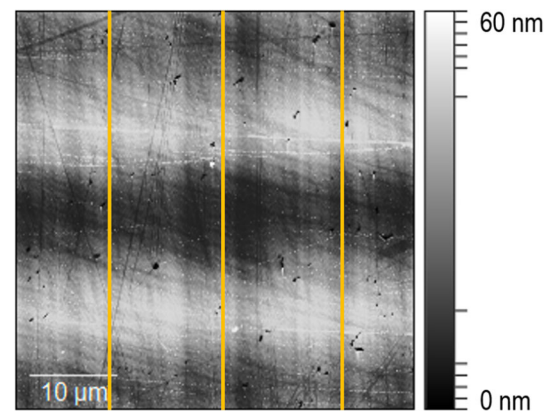
**Fig. 3** Optical micrograph of a 12-line grating obtained by 9 MeV C ion irradiation. Line spacing is  $20\ \mu\text{m}$ , and the overall grating width is  $250\ \mu\text{m}$



**Fig. 4** 3D image scan as measured by AFM of the grating obtained by 9 MeV C ion irradiation



**Fig. 5** 2D image scan ( $45 \times 45\ \mu\text{m}$ ) as measured by AFM of the grating obtained by 9 MeV C ion irradiation. Scanning direction is conducted along the grating dispersive direction, perpendicular to the grating lines



implanted in diamond. Hence, we conclude that its contribution to the pattern smoothing is minor, compared to the beam size and material properties. Moreover, since the beam width is very small along the  $x$ -axis, the dominating effect is expected to come from the elastic response of the material. This effect has been modeled in a preliminary way by convoluting a swelling profile of the type depicted in Fig. 1 to a Gaussian profile. A fair agreement between model and AFM data is obtained by setting the period to  $20\ \mu\text{m}$ , choosing a sigma of  $3.7\ \mu\text{m}$  for the Gaussian and a slope of  $0.925^\circ$ , as may be seen in Fig. 7, where the ideal grating profile, the one calculated after convolution, and the AFM data are plotted together for comparison.

A detailed study of the contribution of material elastic effects is outside the scope of this paper. As a preliminary test, finite element (FE) simulations were performed with the aim of justifying the approach taken to use the ideal swelling profile convoluted to a Gaussian with the proper width to describe the data. The simulations were performed using COMSOL Multiphysics considering a representative  $80$  by  $60$  by  $10\ \mu\text{m}^3$  diamond volume, in which  $20$  by  $60$  by  $10\ \mu\text{m}^3$  subvolumes represent the individual implanted regions. The implantation swelling mechanism is simulated by introducing residual stresses in a substrate with spatially variable density and mechanical properties due to irradiation and evaluating deformation and internal strains after relaxation. This model has been presented and validated experimentally in previous works ([4–8, 19]) Material parameters are: diamond density  $\rho_d =$



**Fig. 6** Three AFM line scans along the grating-dispersive direction (taken vertically from top to bottom in Fig. 5, orange solid lines) are shown, as a demonstration of the reproducibility of the manufacturing method. Different symbols and colors are used for the three scans

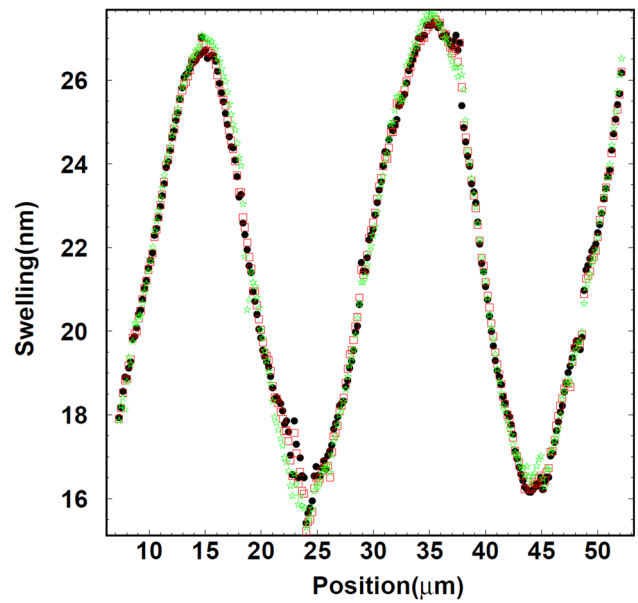
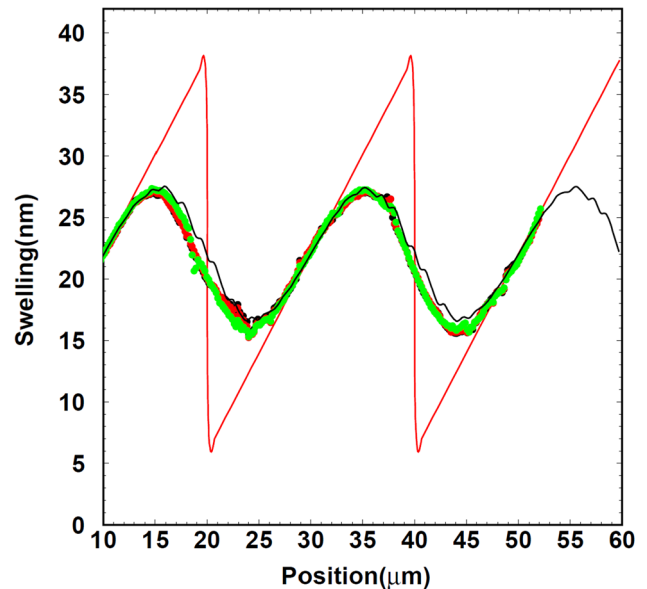


**Fig. 7** Three AFM line scans (solid circles) compared to the ideal grating profile (red line) with a slope of 0.0925° and the smoothed-out profile obtained by convoluting to a Gaussian of sigma 3.7 μm. Both the slope and Gaussian width value have been chosen to get the best agreement between calculation and experimental data



3515 kg/m<sup>3</sup>, amorphous (implanted) carbon density  $\rho_{aC} = 2060 \text{ kg/m}^3$ , diamond Young’s modulus  $E_d = 1220 \text{ GPa}$ , and amorphous carbon Young’s modulus  $E_{aC} = 21.38 \text{ GPa}$ . The density of the implanted region is calculated as [19]

$$\rho(y) = \rho_d - (\rho_d - \rho_{aC}) \cdot \left( 1 - \exp \left[ -\frac{\Phi \cdot \lambda(y)}{\gamma(1 - \rho_{aC}/\rho_d)} \right] \right) \tag{4}$$

where  $\gamma = 1.77 \times 10^{23} \text{ cm}^{-3}$  is the atomic density of diamond,  $\Phi$  is the implantation fluence, and  $\lambda(y)$  is the linear vacancy density, as derived from SRIM. Equation (4) accounts for defect recombination and damage saturation effects in the crystal, and a similar functional dependence is assumed for the Young’s modulus and Poisson’s ratio variation [19].

Consider a small cubic volume  $V$  of side  $l$ , located at a point  $(x, y, z)$  in the irradiated diamond substrate. If unconstrained, it expands upon irradiation to a cubic volume  $V_f$  of side  $(l + \Delta l)$ . The new volume is inversely proportional to the new density:

$$\frac{\rho_d}{\rho(x, y, z)} = \frac{V_f}{V} = \frac{(l + \Delta l)^3}{l^3} = \left( \frac{l + \Delta l}{l} \right)^3 = (1 + \varepsilon_r(x, y, z))^3 \tag{5}$$

**Fig. 8** Finite element analysis calculation of the grating topography with the irradiation conditions used in the experiment, as detailed in Sect. 4

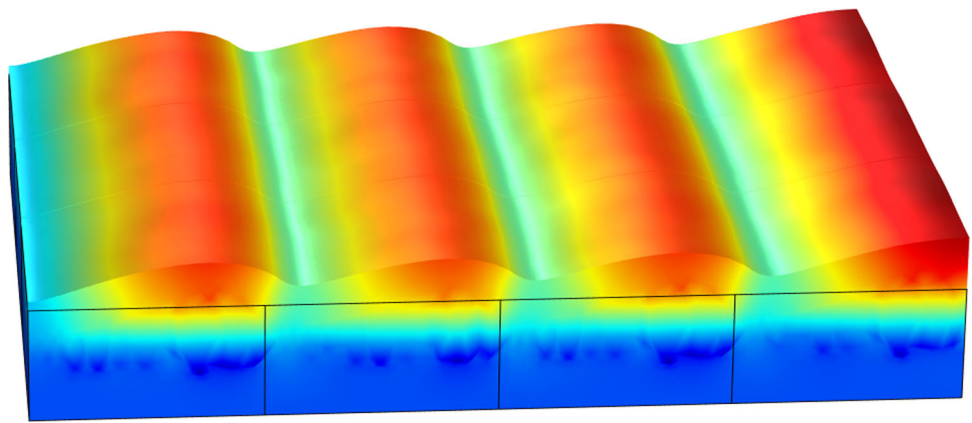
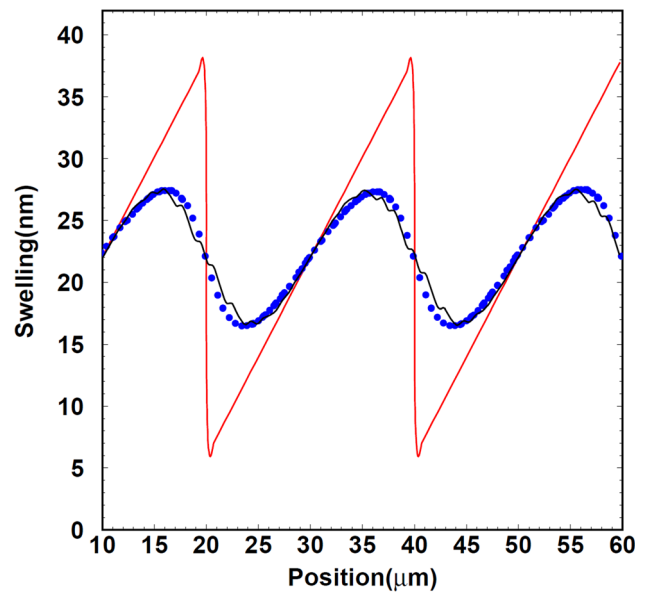


**Fig. 9** Ideal grating profile with a slope value of 0.0925° (red line), profile smoothed out by convolution to a Gaussian of sigma 3.7 μm (black line) and finite element calculation of the material response (blue solid circles)



Hence, the non-uniform density variation causes a lattice mismatch in adjacent layers of the material. Imposing continuity of displacements amounts to imposing as inputs residual strains of amplitude  $\epsilon_r$  at the point  $(x, y, z)$ , given by [19]

$$\epsilon_r(y) = \sqrt[3]{\frac{\rho_d}{\rho(y)}} - 1 \tag{6}$$

where  $y$  is the vertical (irradiation) direction. This produces an observable surface swelling varying between about 15 and 25 nm on the surface of the irradiated samples. Figure 8 provides the swelling profile as predicted by this simulation. Figure 9 compares the simulated profile, plotted as a line scan, as compared to the ideal profile convoluted to a Gaussian of width 3.7 μm, as determined by comparison with the data. In both cases, the fluence irradiation profile has been calculated assuming the 0.925° value, as determined by comparing with experimental data. The agreement of the two models is excellent.

It is clear from the data obtained that the process is very reproducible, and the dose deposition patterns may be easily renormalized to accurately fine tune the desired blaze angle value, even for very low angles, which are particularly challenging with traditional grating manufacturing technologies. On the other hand, the preliminary evaluation of elastic effects made here sets a limit to the line density practically achievable with this technique, due to the smoothing of the grating profile. The functionality of the grating, when the periodicity of the lines is according to specification, depends on the total fraction of the area where the surface has the nominal slope. Therefore, the main effect of smoothing is a decrease in the grating efficiency. Whereas a quantitative evaluation of the grating efficiency for the smoothed geometries herein obtained is outside the scope of this work, it is clear by inspecting Fig. 6 that a substantial part of the grating has a well-defined slope and that the smoothening of the tip for each grating line affects a limited fraction of the area. On the other hand, sawtooth profiles with periods shorter than 20 μm are expected to produce gratings where the smoothing becomes a very important limitation. Future works are foreseen to explore the limit of shorter periods with new experiments, to confirm these preliminary conclusions.

## 5 Conclusions and outlook

A novel manufacturing scheme has been designed, allowing to manufacture mechanical gratings in single-crystal diamond via swift heavy-ion irradiation. Practical implementation details have been checked with a simplified geometry, inspired in the LOREA beamline at ALBA. The results of the experiment have been positive, validating the conceptual approach and opening up the possibility to consider upscaling of this strategy. The main challenges for such upscaling are indicated as follows:

- The total irradiation time with our experimental setup and with our choice of ion species and energy was a few hours for only 12 grating lines. Whereas different aspects of the process, as the time overhead of our beam scanning system when changing direction at the end of each scanning line, may lead to a significant gain in efficiency, still the total time required for a grating of several mm length is foreseen to be in the range of several tens of hours. Some alternatives to this bottleneck may imply exploring different (heavier) ion species, as the same level of damage is then obtained with lower fluences. Silicon or gold may be cases to be explored.
- The elastic response of the material makes a significant contribution to the pattern smoothing. This becomes a limitation if shorter grating periods are desired. As a preliminary conclusion, we consider that 20- $\mu\text{m}$ -period gratings may be manufactured with a very limited impact for efficiency due to smoothing, whereas shorter periods would incur in efficiency problems.
- As indicated above, the total size of the diamond samples available commercially at a reasonable price is for the moment a clear limitation for actual operational gratings in the soft X-ray regime.

Thus, this paper provides useful indications on how to progress and opens alternative routes to the state-of-the art grating manufacturing methodologies, fostering opportunities for open innovation.

**Acknowledgements** The authors acknowledge funding support by the following projects: PID2020-112770RB-C22 from the Spanish Ministry of Science and Innovation, TechnoFusión (III)-CM (S2018/EMT-4437) from Comunidad de Madrid (cofinanced by ERDF and ESF), agreement between Community of Madrid and Universidad Autónoma de Madrid (item “Excellence of University Professorate”). M.L.C. acknowledges financial support from the research project “Captación de Talento UAM” Ref: #541D300 supervised by the Vice-Chancellor of Research of Universidad Autónoma de Madrid (UAM). LOREA beamline at ALBA is a project co-funded by the European Regional Development Fund (ERDF) within the Framework of the Smart Growth Operative Programme 2014-2020. The authors acknowledge the support from The Centro de Microanálisis de Materiales (CMAM)—Universidad Autónoma de Madrid, for the beam time proposal (demonstration of a grating profile for soft X-rays in diamond via ion lithography) with code IuB-005/21, and its technical staff for their contribution to the operation of the accelerator. We also acknowledge P. Olivero for very useful comments on the manuscript draft.

**Funding** Open Access funding provided thanks to the CRUE-CSIC agreement with Springer Nature.

**Data Availability Statement** This manuscript has associated data in a data repository. [Authors’ comment: Data are foreseen to be uploaded to Zenodo and will be made available on the basis of reasonable request.]

**Open Access** This article is licensed under a Creative Commons Attribution 4.0 International License, which permits use, sharing, adaptation, distribution and reproduction in any medium or format, as long as you give appropriate credit to the original author(s) and the source, provide a link to the Creative Commons licence, and indicate if changes were made. The images or other third party material in this article are included in the article’s Creative Commons licence, unless indicated otherwise in a credit line to the material. If material is not included in the article’s Creative Commons licence and your intended use is not permitted by statutory regulation or exceeds the permitted use, you will need to obtain permission directly from the copyright holder. To view a copy of this licence, visit <http://creativecommons.org/licenses/by/4.0/>.

## References

1. F. Agulló-López, A. Climent-Font, A. Muñoz-Martín, J. Olivares, A. Zucchiatti, *Prog. Mater. Sci.* **76**, 1 (2016). <https://doi.org/10.1016/j.pmatsci.2015.06.002>
2. F. Picollo, D. Gatto Monticone, P. Olivero, B.A. Fairchild, S. Rubanov, S. Prawer, E. Vittone, *New J. Phys.* **14**, 053011 (2012). <https://doi.org/10.1088/1367-2630/14/5/053011>
3. G. García, M. Díaz-Hijar, V. Tormo-Márquez, I. Preda, O. Peña-Rodríguez, J. Olivares, *Diam. Relat. Mater.* **58**, 226 (2015). <https://doi.org/10.1016/j.diamond.2015.08.014>
4. M. Piccardo, F. Bosia, P. Olivero, N. Pugno, *Diam. Relat. Mater.* **48**, 73 (2014). <https://doi.org/10.1016/j.diamond.2015.08.014>
5. F. Bosia, S. Calusi, L. Giuntini, S. Lagomarsino, A. Lo Giudice, M. Massi, P. Olivero, F. Picollo, S. Sciortino, A. Sordini, M. Vannoni, E. Vittone, *Nucl. Instrum. Methods Phys. Res. B* **268**, 2991 (2010). <https://doi.org/10.1016/j.nimb.2010.05.025>
6. F. Bosia, N. Argiolas, M. Bazzan, P. Olivero, F. Picollo, A. Sordini, M. Vannoni, E. Vittone, *Diam. Relat. Mater.* **20**, 774 (2011). <https://doi.org/10.1016/j.diamond.2011.03.025>
7. F. Bosia, N. Argiolas, M. Bazzan, B.A. Fairchild, A.D. Greentree, D.W.M. Law, P. Olivero, F. Picollo, S. Rubanov, S. Prawer, *J. Phys. Condens. Matter* **25**, 385403 (2013). <https://doi.org/10.1088/0953-8984/25/38/385403>
8. G. García, I. Preda, M. Díaz-Hijar, V. Tormo-Márquez, O. Peña-Rodríguez, J. Olivares, F. Bosia, N.M. Pugno, F. Picollo, L. Giuntini, A. Sordini, P. Olivero, L. López-Mir, C. Ocal, *Diam. Relat. Mater.* **69**, 1 (2016). <https://doi.org/10.1016/j.diamond.2016.06.015>
9. A.L. Stepanov, V.I. Nuzhdin, M.F. Galyautdinov, N.V. Kurbatova, V.F. Valeev, Y.N. Osin, *Tech. Phys. Let.* **43**, 104 (2017). <https://doi.org/10.1134/S1063785017010266>
10. W.B. Peatman, *Gratings, mirrors and slits: beamline design for soft X-ray synchrotron radiation sources* (CRC Press, Berlin, 1997)
11. S. Mobilio, F. Boscherini, C. Menaghini, *Synchrotron radiation: basics, methods and applications* (Springer, Heidelberg, 2015)
12. BL20-LOREA at ALBA synchrotron, <https://www.albasynchrotron.es/en/beamlines/bl20-lorea>



13. ALBA synchrotron, <https://www.cells.es>
14. F.J. Ziegler, J.P. Biersack, M.D. Ziegler, *The stopping and range of ions in solids* (SRIM Co., Pergamon, New York, 1985)
15. J.F. Ziegler, M.D. Ziegler, J.P. Biersack, Nucl. Instrum. Methods Phys. Res. B **268**, 1818 (2010). <https://doi.org/10.1016/j.nimb.2010.02.091>
16. Element six, <http://www.e6.com/>
17. A. Redondo-Cubero, M.J.G. Borge, N. Gordillo, P.C. Gutiérrez, J. Olivares, R. Pérez Casero, M.D. Ynsa, Eur. Phys. J. Plus **136**, 175 (2021). <https://doi.org/10.1140/epjp/s13360-021-01085-9>
18. M.D. Ynsa, M.A. Ramos, N. Skukan, V. Torres-Costa, M. Jaksic, Nucl. Instrum. Methods Phys. Res. B **348**, 174 (2015). <https://doi.org/10.1016/j.nimb.2014.11.036>
19. A. Battiato, M. Lorusso, E. Bernardi, F. Picollo, F. Bosia, D. Ugues, A. Zelferino, A. Damin, J. Baima, N.M. Pugno, E.P. Ambrosio, P. Olivero, Acta Mater. **116**, 95 (2016). <https://doi.org/10.1016/j.actamat.2016.06.019>